Imaging, Diagnosis, Prognosis

Clinical Cancer Research

2-(3-{1-Carboxy-5-[(6-[^{18}F]Fluoro-Pyridine-3-Carbonyl)-Amino]-Pentyl}-Ureido)-Pentanedioic Acid, [^{18}F]DCFPyL, a PSMA-Based PET Imaging Agent for Prostate Cancer

Ying Chen[1], Mrudula Pullambhatla[1], Catherine A. Foss[1], Youngjoo Byun[1,2], Sridhar Nimmagadda[1], Srinivasan Senthamizhchelvan[1], George Sgouros[1], Ronnie C. Mease[1], and Martin G. Pomper[1]

Abstract

Purpose: We have synthesized and evaluated *in vivo* 2-(3-{1-carboxy-5-[(6-[^{18}F]fluoro-pyridine-3-carbonyl)-amino]-pentyl}-ureido)-pentanedioic acid, [^{18}F]DCFPyL, as a potential imaging agent for the prostate-specific membrane antigen (PSMA). PSMA is upregulated in prostate cancer epithelia and in the neovasculature of most solid tumors.

Experimental Design: [^{18}F]DCFPyL was synthesized in two steps from the *p*-methoxybenzyl (PMB) protected lys-C(O)-glu urea precursor using 6-[^{18}F]fluoronicotinic acid tetrafluorophenyl ester ([^{18}F]F-Py-TFP) for introduction of ^{18}F. Radiochemical synthesis was followed by biodistribution and imaging with PET in immunocompromised mice using isogenic PSMA PC3 PIP and PSMA- PC3 flu xenograft models. Human radiation dosimetry estimates were calculated using OLINDA/EXM 1.0.

Results: DCFPyL displays a K_i value of 1.1 ± 0.1 nmol/L for PSMA. [^{18}F]DCFPyL was produced in radiochemical yields of 36%–53% (decay corrected) and specific radioactivities of 340–480 Ci/mmol (12.6–17.8 GBq/μmol, $n = 3$). In an immunocompromised mouse model [^{18}F]DCFPyL clearly delineated PSMA+ PC3 PIP prostate tumor xenografts on imaging with PET. At 2 hours postinjection, 39.4 ± 5.4 percent injected dose per gram of tissue (%ID/g) was evident within the PSMA+ PC3 PIP tumor, with a ratio of 358:1 of uptake within PSMA+ PC3 PIP to PSMA− PC3 flu tumor placed in the opposite flank. At or after 1 hour postinjection, minimal nontarget tissue uptake of [^{18}F]DCFPyL was observed. The bladder wall is the dose-limiting organ.

Conclusions: These data suggest [^{18}F]DCFPyL as a viable, new positron-emitting imaging agent for PSMA-expressing tissues. *Clin Cancer Res; 17(24); 7645–53. ©2011 AACR.*

Introduction

Prostate cancer (PCa) is the second leading cause of death from cancer in men in the United States (1). The vast majority of men dying of PCa succumb to metastatic, castration-resistant disease. Among the reasons to image PCa, including initial staging, therapeutic monitoring, guiding focal therapies, and determining the location of recurrence after prostatectomy, one elusive but important goal is to image with a view to distinguishing indolent from aggressive disease. Although no single marker is capable of providing that distinction, the prostate-specific membrane antigen (PSMA), a type II integral membrane protein overexpressed on prostate tumors, provides a step in that direction. Both disease-free survival and time to prostate-specific antigen (PSA) progression are decreased in patients with elevated levels of PSMA within their tumors (2, 3). PSMA expression has long been associated with androgen-independent disease (4). Recently, Evans and colleagues showed that a positron-emitting version of the anti-PSMA monoclonal antibody (mAb) J591 (5) was able to leverage PSMA expression into a noninvasive biomarker of androgen receptor (AR) signaling (6).

Several modalities have been applied to imaging PCa, but to study PSMA at high sensitivity *in vivo* others and we have focused on the radionuclide and optical molecular imaging techniques (7–18). PCa has not succumbed as readily to molecular imaging as other solid tumors as it is not easily visualized on positron emission tomography (PET) with [^{18}F]fluorodeoxyglucose (FDG), the clinical gold standard, because PCa tends to grow slowly and is less metabolically active with respect to glucose transport and consumption. Another difficulty in imaging PCa with FDG, or any other radiopharmaceutical that is excreted through the urine, is the proximity of the prostate to the urinary bladder, which can obscure specific binding to intraprostatic PCa. There are ways around that problem, including rapid scanning soon after voiding (before accumulation of radiotracer within the

Authors' Affiliations: [1]Russell H. Morgan Department of Radiology and Radiological Science, Johns Hopkins Medical School, Baltimore, Maryland; and [2]College of Pharmacy, Korea University, Sejong-ro, Jochiwon-eup, Yeongi-gun, Chungnam, South Korea

Corresponding Author: Martin G. Pomper, Johns Hopkins Medical School, 1550 Orleans Street, 492 CRB II. Phone: 410-955-2789; Fax: 443-817-0990; E-mail: mpomper@jhmi.edu

doi: 10.1158/1078-0432.CCR-11-1357

Translational Relevance

Relative to other malignancies, prostate cancer (PCa) is an elusive target for molecular imaging. By targeting the prostate-specific membrane antigen (PSMA), [^{18}F]DCFPyL may provide insight into prognosis and androgen receptor (AR) signaling–an important target in PCa research–as well as a way to image locally invasive disease and metastases. The initial indications for [^{18}F]DCFPyL will be in staging of patients with PCa diagnosed at biopsy or who present with a rising prostate-specific antigen (PSA) blood test after prostatectomy. Other indications include therapeutic monitoring in the context of standard chemotherapeutic agents, AR-based agents and possibly for emerging PSMA-based therapeutics. The superior pharmacokinetics of this compound, namely the high uptake in tumor versus nontarget tissues, the fact that it is a low molecular weight agent, that it can be radiolabeled with a widely available isotope (^{18}F), and its tractable radiation dosimetry profile all point toward rapid clinical translation through the exploratory Investigational New Drug (eIND) mechanism.

bladder), catheterization, and application of postprocessing techniques (19). Accordingly, a variety of radiopharmaceutical imaging agents have been developed for PCa, including radiolabeled versions of choline (20, 21), [^{11}C]acetate (22–24), 1-amino-3-[^{18}F]fluorocyclobutane-1-carboxylic acid ([^{18}F]FACBC; 25), as well as a variety of radiolabeled antibodies specific for PSMA (6, 26–29), with several beginning to be seen in clinical trials.

We have previously reported the development of *N*-[*N*-[(*S*)-1,3-dicarboxypropyl]carbamoyl]-4-[^{18}F]fluorobenzyl-L-cysteine, [^{18}F]DCFBC (9), with which we have initiated a phase 1 trial (30). [^{18}F]DCFBC showed 8% injected dose per gram (%ID/g) within PSMA+ PIP tumor, achieved at 60 minutes after injection, which decreased to 4.7% at 2 hours postinjection. Nearly 2% ID/g in bone was present at most time points. To improve upon the pharmacokinetics of [^{18}F]DCFBC, we have now synthesized 2-(3-{1-carboxy-5-[(6-[^{18}F]fluoro-pyridine-3-carbonyl)-amino]-pentyl}-ureido)-pentanedioic acid, [^{18}F]DCFPyL ([^{18}F]**3**), which uses the lys-C(O)-glu motif and contains a [^{18}F]fluoropyridyl substituent, in analogy to a radioiodinated PSMA-binding ligand that we previously reported, which showed high uptake within PSMA+ tumor and fast clearance from nontarget tissues (11).

Results

Chemical and radiochemical syntheses

The tosylate salt of **1**, previously described by us (10), was reacted with F-Py-TFP (31) to generate fluoropyridyl urea **2**. Deprotection afforded DCFPyL (**3**) in 81% yield (Fig. 1). The ^{18}F-labeled prosthetic group [^{18}F]F-Py-TFP was prepared by a literature procedure (31) and used to generate [^{18}F]DCFPyL ([^{18}F]**3**; Fig. 1). The decay-corrected radiochemical yields of [^{18}F]**3** ranged from 36%–53% based on starting [^{18}F]F$^-$ ($n = 3$) with absolute yields of 7.7–10.4 mCi (285–385 MBq) after HPLC purification. The mean synthesis time was 128 minutes from the time of addition of [^{18}F]F$^-$. Starting from 44–61 mCi (1,628–2,257 MBq) of [^{18}F]F$^-$, the specific radioactivity of [^{18}F]**3** ranged from 340–480 Ci/mmol (12.6–17.8 GBq/μmol).

PSMA inhibition assay

The K_i value for **3** was determined using a modification of the Amplex Red glutamic acid assay (32). The K_i value for **3** was 1.1 ± 0.1 nmol/L, comparable with that of ZJ-43, which is 1.4 ± 0.2 nmol/L when used as an internal reference.

Biodistribution

Compound [^{18}F]**3** was assessed for its *ex vivo* pharmacokinetics in nonobese diabetic severe-combined immunodeficient (NOD-SCID) mice bearing both PSMA+ PC3-PIP and PSMA− PC3-flu xenografts. Table 1 shows the %ID/g of radiochemical in selected organs. Compound [^{18}F]**3** showed clear PSMA-dependent uptake within PSMA+ PC3 PIP xenografts, reaching a value of 46.7 ± 5.8%ID/g at 30 minutes postinjection (p.i.), which decreased by only about 10% over the ensuing 4 hours. At 60 minutes p.i. the kidney, liver, and spleen displayed the highest uptake. By that time, the urinary bladder also showed relatively high uptake. However, that uptake includes excretion at all time points. Rapid clearance from the kidneys was shown, decreasing from 74.1 ± 6.6%ID/g at 30 minutes to 7.4 ± 0.9%ID/g at 4 hours. The relatively high values noted in kidney are partially due to high expression of PSMA within proximal renal tubules (33, 34). The ratio of uptake within PSMA+ PIP to PSMA− flu tumors ranged from 40:1 to more than 1,000:1 over the 4-hour time period of the study. A possible explanation for that increased tumor uptake of radiochemical over time could be due to ligand-mediated PSMA internalization within tumor cells (35, 36). Less retention in kidney relative to tumor over time could be due to a lower degree of internalization in this (normal) tissue and/or different metabolism of [^{18}F]**3**, which does not promote retention of radiochemical in kidney. Relatively low bone uptake (<1% ID/g at all time points) suggests little metabolic defluorination of [^{18}F]**3**.

Small animal PET imaging

Intense radiochemical uptake was seen only in the kidneys and PSMA+ PC3 PIP tumor after administration of [^{18}F]**3** (Fig. 2). As noted above for the *ex vivo* study, the intense renal uptake was partially due to specific binding of the radiotracer to proximal renal tubules (33, 34) and to excretion of this hydrophilic compound. By 3.5 hours after njection, only the PSMA+ tumor is visible with no

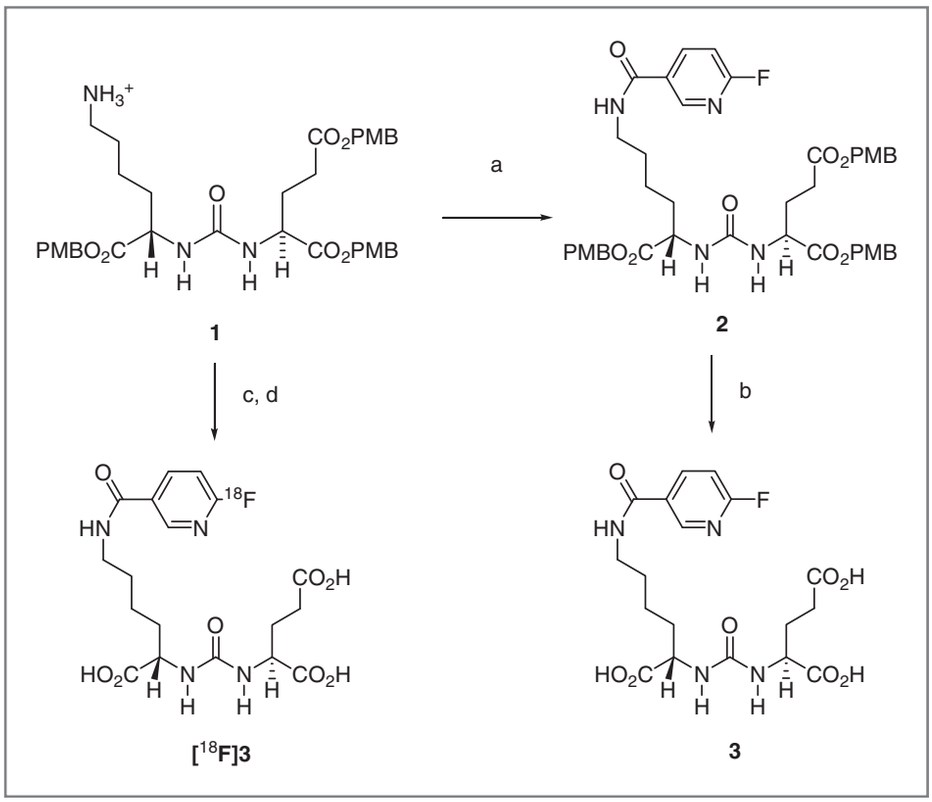

Figure 1. Synthesis of DCFPyL **3** and [^{18}F]DCFPyL [^{18}F]**3**. (a) 6-Fluoro-nicotinic acid-2,3,5,6-tetrafluoro-phenyl ester, Et_3N, CH_2Cl_2; (b) TFA/CH_2Cl_2; (c) 6-[^{18}F]fluoro-nicotinic acid-2,3,5,6-tetrafluoro-phenyl ester; (d) TFA/anisole.

radiochemical background in liver or the gastrointestinal tract to obscure potential metastases.

Human radiation dosimetry estimates

Table 2 lists source organ time-integrated activity coefficients for [^{18}F]**3**. Table 3 lists target organ absorbed doses. The organ with the highest mean absorbed dose per unit administered activity was the urinary bladder wall, 0.15 mGy/MBq, followed by the kidneys at 0.05 mGy/MBq. The absorbed dose to tissues listed in Table 3 that were not assigned a time-integrated activity coefficient reflects cross-fire photon contribution from organs that were assigned a

Table 1. Biodistribution of [^{18}F]**3** in tumor-bearing mice[a]

Organ	30 min	60 min	120 min	240 min
Blood	1.53 ± 0.19	0.24 ± 0.05	0.43 ± 0.37	0.03 ± 0.01
Heart	0.68 ± 0.07	0.20 ± 0.11	0.06 ± 0.01	0.02 ± 0.00
Lung	1.91 ± 0.47	0.55 ± 0.17	0.18 ± 0.02	0.06 ± 0.00
Liver	3.88 ± 0.74	2.87 ± 0.92	2.14 ± 0.11	1.80 ± 0.39
Stomach	1.50 ± 1.12	0.35 ± 0.34	0.08 ± 0.03	0.02 ± 0.00
Pancreas	1.02 ± 0.53	0.26 ± 0.13	0.08 ± 0.00	0.03 ± 0.01
Spleen	7.59 ± 3.56	2.70 ± 1.28	0.69 ± 0.11	0.23 ± 0.09
Kidney	74.1 ± 6.6	42.3 ± 19.0	15.7 ± 3.3	7.42 ± 0.89
Muscle	0.39 ± 0.05	0.61 ± 0.92	0.04 ± 0.00	0.05 ± 0.05
Bone	0.82 ± 0.16	0.42 ± 0.15	0.33 ± 0.08	0.43 ± 0.06
sm. Intest	0.79 ± 0.11	0.31 ± 0.12	0.11 ± 0.07	0.05 ± 0.01
lrg. Intest	0.73 ± 0.04	0.40 ± 0.17	0.12 ± 0.05	0.06 ± 0.01
Bladder (empty)	18.6 ± 18.1	9.88 ± 4.92	6.44 ± 4.42	1.54 ± 1.79
PSMA+ PIP	46.7 ± 5.8	44.2 ± 9.7	39.4 ± 5.4	36.6 ± 4.3
PSMA$^-$flu	1.17 ± 0.41	0.36 ± 0.14	0.11 ± 0.02	0.03 ± 0.01
PIP/flu	40	123	358	1220

[a]Values are in% ID/g SD; $n = 4$.

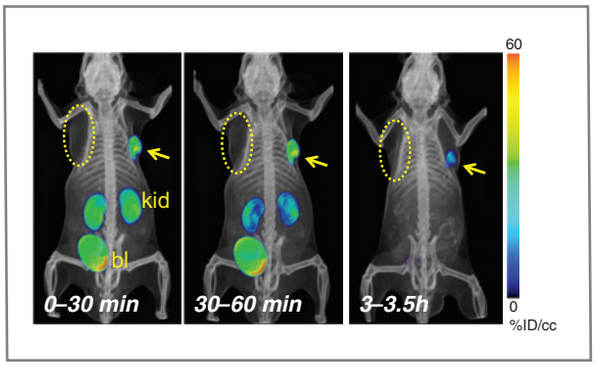

Figure 2. PET-CT volume-rendered composite images representing the time course of radiochemical uptake after administration of [^{18}F]**3**. PSMA+ PC3 PIP (arrow) and PSMA- PC3 flu (dotted oval) tumors are present in subcutaneous tissues posterior to opposite forearms, as indicated. The mouse was injected intravenously with 0.38 mCi (14.1 MBq) [^{18}F]**3** at Time 0. By 30 minutes postinjection radiochemical uptake was evident within the PIP tumor and kidneys. Radioactivity receded from kidneys faster than from tumor, and was not evident within kidneys by 3.5 hours postinjection. Radioactivity within bladder was due to excretion. At no time was radiochemical clearly visualized within the flu tumor. kid = kidneys, bl = urinary bladder.

time-integrated activity coefficient and contribution from radioactivity assigned to the remainder of the body. The effective dose based on the ICRP 60 tissue weighting factors was 13.6 μSv/MBq. On the basis of the dosimetry results a maximum of 9 mCi (331 MBq) can be administered without exceeding the 50 mGy critical organ dose limit (urinary bladder wall in this case), for a single administration of radioactive material for research use as specified in Code of Federal Regulations 21, part 361.

Discussion

A variety of positron-emitting agents–as well as other techniques and modalities–for imaging PCa have been developed and have recently been reviewed elsewhere (37–39). With respect to PSMA specifically, in addition to imaging *per se*, PSMA affinity agents, such as low molecular weight compounds (40), antibodies (41) and aptamers (42), have been conjugated to and used to target nanoparticles and to deliver shRNA (43) to PSMA+ cells and tissues. Because PSMA is expressed in most solid tumor neovasculature (44–47), it may be used in principle as a general tumor imaging target with one clinical trial showing imaging of nonprostate tumors (29). However, as stated at the outset, the main value of a PSMA-based imaging agent may be in providing an avenue through which to begin determining the aggressiveness of an individual prostate tumor. Furthermore, PSMA may also be used as an indicator of AR signaling within prostate tumors (6, 48, 49), which would provide a particularly important function for a PSMA-based imaging agent as new AR-targeted drugs emerge (50). In this regard, targeting PSMA may provide more information than targeting AR directly with an agent such as [^{18}F]fluordihydrotestosterone ([^{18}F]FDHT; ref. 51), as the AR will be occupied in patients treated with AR-based therapeutics. Positron-emitting progestins have been pursued as imaging agents for breast cancer for similar reasons

Table 2. Human source organ time-integrated activity coefficients

Source organ	Time-integrated activity coefficient (MBq-h/MBq)
Lower large intestine	4.23E-04
Small intestine	1.30E-03
Stomach	3.36E-04
Upper large intestine	4.23E-04
Heart wall	3.97E-04
Kidneys	7.47E-02
Liver	4.09E-02
Lungs	3.52E-03
Muscle	4.50E-02
Pancreas	1.48E-04
Spleen	2.98E-03
Urinary bladder contents	3.09E-01
Remainder	8.51E-01

Table 3. Estimated human organ absorbed dose

Target organ	Absorbed dose (mGy/MBq)
Adrenals	6.46E-03
Brain	4.84E-03
Breasts	3.97E-03
Gallbladder wall	6.48E-03
Lower large intestine wall	9.40E-03
Small intestine	7.53E-03
Stomach wall	5.27E-03
Upper large intestine wall	6.67E-03
Heart wall	3.26E-03
Kidneys	4.81E-02
Liver	7.38E-03
Lungs	3.01E-03
Muscle	3.95E-03
Ovaries	9.06E-03
Pancreas	4.38E-03
Red marrow	5.35E-03
Osteogenic cells	7.59E-03
Skin	3.84E-03
Spleen	6.57E-03
Testes	7.06E-03
Thymus	4.43E-03
Thyroid	4.45E-03
Urinary bladder wall	1.51E-01
Uterus	1.45E-02
Total body	5.71E-03
Effective dose equivalent (mSv/MBq)	1.80E-02
Effective dose (mSv/MBq)	1.36E-02

(52), namely, that estrogen receptor, the target for [^{18}F]fluoroestradiol, is largely occupied in patients undergoing antiestrogen therapy.

Among the positron emitting isotopes that are integrated into tumor-targeting agents of low molecular weight, including ^{11}C, ^{18}F, ^{64}Cu, ^{86}Y, ^{89}Zr, and ^{124}I, ^{18}F is considered a particularly convenient radionuclide because of its nearly pure positron emission, isosterism with hydrogen, relative ease of incorporation into relevant affinity reagents at high specific radioactivity through $^{18}F^-$ or a variety of prosthetic groups (as described here), and its relatively long physical half-life (110 min) enabling shipment of ^{18}F-labeled radiotracers to sites distant from their production. Carbon-11-labeled PET agents are becoming increasingly viewed as being for proof-of-principle, with commercial entities showing interest primarily in those labeled with ^{18}F, particularly for indications outside of the central nervous system (CNS). The pharmacokinetics of most agents for use outside of the CNS, particularly those of low molecular weight, are more amenable to an ^{18}F radiolabel than to ^{11}C, which may not have a sufficiently long physical half-life to enable washout from nontarget sites during the imaging study. For those reasons, we have chosen to focus on development of a new ^{18}F-labeled PSMA imaging agent for PET.

Antibodies (6, 27, 53) and antibody fragments (54), aptamers (55), and low molecular weight PSMA-binding affinity agents (9, 13, 18, 56, 57) have recently been derivatized with positron-emitting isotopes. Those agents will have different indications, as they have widely varying pharmacokinetics, however, each class has shown PSMA-specific binding in preclinical studies. In terms of specific, *in vivo* target tumor to nontarget tumor uptake ratio, the radiolabeled mAbs ^{64}Cu-DOTA-3/A12 (53) and ^{89}Zr-DFO-J591 (27) both showed values of approximately 3:1 at 48 hours postinjection. But comparisons are difficult due to the differences in tumor models used and, importantly, the variable degree of PSMA expressed within them. Antibodies may have an advantage over agents of lower molecular weight due to their putative inaccessibility to apically positioned PSMA on nonmalignant cells (27), suggesting enhanced tumor specificity for mAbs. PSMA-directed mAb fragments have not yet shown selective uptake in PSMA-expressing tumors *in vivo* (54).

Among nonprotein-based PET imaging agents for PSMA, Rockey and colleagues have optimized conditions for conjugating ^{64}Cu to a PSMA-targeting aptamer, which has shown PSMA-mediated uptake in PSMA+ 22RV1 prostate tumor cells relative to PSMA- PC3 cells (55). So far low molecular weight imaging agents for PSMA fall into 2 classes, the ureas, such as [^{18}F]**3**, and the phosphoramidates (18). Both have a terminal glutamate at the P1′ position, which enables productive binding to PSMA. Both are amenable to modification with bulky substituents that interact with the arginine patch or tunnel region on PSMA (58–60). In addition to ^{18}F, the urea-based compounds have been functionalized with ^{11}C (56) and ^{68}Ga (13) for PET. A phosphoramidate has been radiolabeled with ^{18}F and tested *in vivo* (18). As suggested above, it is challenging to compare the pharmacokinetics of these compounds because of the different models used between investigators and even within the same research group, due to the variable expression of PSMA between experiments within what is considered a PSMA+ cell line. For example, the PSMA+ PC3-PIP cell line expresses significantly lower PSMA than does PSMA+ LNCaP (61). However, we prefer the isogenic PSMA+ PIP versus PSMA− flu comparison as the 2 cell lines are phenotypically identical, differing only in PSMA expression. We have also found that the PSMA+ PC3 PIP cells can lose PSMA expression after several passages. With those caveats in mind, [^{18}F]**3** shows 39.4% ID/g in PSMA+ PIP tumor with a PIP:flu uptake ratio of 358 at 2-hour postinjection, while the ^{18}F-labeled phosphoramidate showed 1.2% ID/g in LNCaP with an LNCaP:PC3 of 3.5 (18). However, renal and liver values for [^{18}F]**3** were higher than for the ^{18}F-labeled phosphoramidate, at 15.7 versus 2.2% and 2.1 versus 0.2%, respectively. [^{18}F]**3** also compares favorably with the first generation ^{18}F-labeled urea, [^{18}F]DCFBC (9), showing an 8-fold higher tumor uptake at 2-hour postinjection. That is important because [^{18}F]DCFBC has proved capable of delineating metastases from prostate cancer in human subjects in a recent first-in-human trial (30).

Conclusions

Patterned after our previously reported radioiodinated PSMA-binding radiotracer that showed high uptake within PSMA+ tumor and fast clearance from nontarget tissues (11), [^{18}F]**3** showed high tumor and low normal tissue uptake and retention in PSMA+ PC3 PIP prostate tumor xenografts. The pharmacokinetics of [^{18}F]**3** compare favorably with other low molecular weight agents that bind PSMA selectively. The preclinical results obtained with [^{18}F]**3** warrant its further pursuit in a variety of clinical scenarios to help localize PCa.

Experimental Section

General procedures

All reagents and solvents were purchased from either Sigma-Aldrich or Fisher Scientific. The tosylate salt of **1** was prepared according to a reported procedure (10). ^{1}H NMR spectra were obtained on a Bruker Avance 400 MHz Spectrometer. ESI mass spectra were obtained on a Bruker Esquire 3000 plus system. High-resolution mass spectra (HRMS) were done by the Mass Spectrometry Facility at the University of Notre Dame using ESI by direct infusion on a Bruker micrOTOF-II. High performance liquid chromatography (HPLC) purification of **3** was done on a Waters 625 LC system with a Waters 490E multiwavelength UV/Vis detector.

[^{18}F]Fluoride was produced by 18 MeV proton bombardment of a high pressure [^{18}O]H_2O target using a General Electric PETtrace biomedical cyclotron. Solid-

phase extraction cartridges (C_{18} plus, Sep-Pak) were purchased from Waters Associates. Reverse phase radio-HPLC purification of [^{18}F]**3** was done using a Varian Prostar System with a Bioscan Flow Count PMT radioactivity detector (Varian Medical Systems). Radioactivity was measured in a Capintec CRC-10R dose calibrator. The specific radioactivity was calculated as the radioactivity eluting at the retention time of product during the semi-preparative HPLC purification divided by the mass corresponding to the area under the curve of the UV absorption.

2-(3-{1-carboxy-5-[(6-fluoro-pyridine-3-carbonyl)-amino]-pentyl}-ureido)-pentanedioic acid, 3

To a solution of **1** (0.015 g, 0.018 mmol) in CH_2Cl_2 (1 mL) was added triethylamine (0.010 mL, 0.072 mmol), followed by 6-fluoro-nicotinic acid 2,3,5,6-tetrafluoro-phenyl ester (F-Py-TFP; ref. 31; 0.005 g, 0.017 mmol). After stirring for 2 hours at ambient temperature, the solvent was evaporated. The crude material was purified on a silica column using methanol/methylene chloride (5:95) to afford 0.009 g (65%) of compound **2**. ^{1}H NMR (400 MHz, $CDC1_3$) δ 8.65 (s, 1H), 8.22 (m, 1H), 7.15–7.24 (m, 7H), 6.83–6.97 (m, 7H), 5.35–5.56 (m, 2H), 4.93–5.08 (m, 6H), 4.31–4.35 (m, 2H), 3.76 (m, 9H), 3.31–3.36 (m, 2H), 2.34 (m, 2H), 2.07 (m, 1H), 1.88 (m, 1H), 1.72 (m, 1H), 1.54 (m, 3H), 1.23 (m, 2H). ESI-Mass calcd for $C_{42}H_{48}FN_4O_{11}$ $[M + H]^+$ 803.3 found 802.9.

A solution of TFA in CH_2Cl_2 (1:1, 2 mL) was added to **2** (0.009 g, 0.011 mmol). The mixture was stirred at ambient temperature for 2 hours, then concentrated on a rotary evaporator. The crude material was purified by HPLC [Econosphere C18 10 μ, 250 × 10 mm, H_2O/CH_3CN/TFA (92/8/0.1), 4 mL/min] to afford 0.004 g (0.009 mmol; 81%) of **3**. ^{1}H NMR (400 MHz, D_2O) δ 8.56 (s, 1H), 8.29 (m, 1H), 7.20 (m, 1H), 4.18–4.24 (m, 2H), 3.42 (m, 2H), 2.49 (m, 2H), 2.15 (m, 1H), 1.87–2.00 (m, 2H), 1.64–1.80 (m, 3H), 1.47 (m, 2H). ESI-Mass calcd for $C_{18}H_{24}FN_4O_8$ $[M + H]^+$ 443.2, found 442.9. ESI-HRMS calcd for $C_{18}H_{24}FN_4O_8$ $[M + H]^+$ 443.1573, found 443.1556.

Radiochemistry

2-(3-{1-Carboxy-5-[(6-[^{18}F]fluoro-pyridine-3-carbonyl)-amino]-pentyl}-ureido)-pentanedioic acid, [^{18}F]DCFPyL ([^{18}F]3)

In a vial containing 2 mg (0.002 mmol) of **1** and 0.005 mL of triethylamine was added [^{18}F]F-Py-TFP (31) in 2 mL CH_2Cl_2. The reaction was heated at 45°C for 20 minutes followed by removal of solvent under a stream of nitrogen, addition of 0.1 mL of 3% anisole/TFA and further heating at 45°C for 10 minutes. The final product was obtained after HPLC purification (Econosphere C18 10 μ, 250 × 10 mm, H_2O/CH_3CN/TFA [90/10/0.1], 4 mL/min) at a retention time of approximately 9.5 minutes, and was neutralized with 1 mol/L $NaHCO_3$, concentrated under vacuum to dryness, reconstituted in PBS (pH 7.4) and passed through a 0.22 μm syringe filter into an evacuated sterile vial.

PSMA inhibition assay

Cell lysates of LNCaP cell extracts were incubated with DCFPyL (0.01 nmol/L–100 μmol/L) in the presence of 4 μmol/L NAAG at 37°C for 2 hours. The amount of released glutamate was measured by incubating with a working solution of the Amplex Red glutamic acid kit (Molecular Probes Inc.) at 37°C for 30 minutes. Fluorescence measurements were done with a VICTOR^{3}V multilabel plate reader (Perkin Elmer Inc.), with excitation at 490 nm and emission at 642 nm. Inhibition curves were determined using semi-log plots, and IC_{50} values were determined at the concentration at which enzyme activity was inhibited by 50%. Assays were done in triplicate with the entire inhibition study being repeated at least once to confirm affinity and mode of inhibition. Enzyme inhibitory constants (K_i values) were generated using the Cheng–Prusoff conversion (62, 63). Data analysis was done using GraphPad Prism version 4.00 for Windows (GraphPad Software).

Cell lines and tumor models

LNCaP cells used in the PSMA inhibition assay were obtained from American Type Culture Collection (ATCC) and were maintained as per ATCC guidelines. PC3 PIP (PSMA+) and PC3 flu (PSMA−) cell lines were obtained from Dr. Warren Heston (Cleveland Clinic) and were maintained as previously described (9). Cells were grown to 80%–90% confluence in a single passage before trypsinization and formulation in Hank's balanced salt solution (HBSS, Sigma) for implantation into mice. Animal studies were in compliance with guidelines related to the conduct of animal experiments of the local Animal Care and Use Committee. For biodistribution and imaging studies of [^{18}F]**3**, male NOD-SCID mice (Johns Hopkins University, in-house colony) were implanted subcutaneously with 1×10^6 PSMA+ PC3 PIP and PSMA− PC3 flu cells behind either shoulder. Mice were imaged or used in biodistribution studies when the tumor xenografts reached 3 to 5 mm in diameter.

Biodistribution

PSMA+ PC3 PIP and PSMA− PC3 flu xenograft-bearing SCID mice were injected *via* the tail vein with 100 μCi (3.7 MBq) of [^{18}F]**3**. In each case 4 mice were sacrificed by cervical dislocation at 30, 60, 120, and 240 minutes p.i. The heart, lungs, liver, stomach, pancreas, spleen, kidney, muscle, bone, small and large intestines, urinary bladder, and PC3 PIP and flu tumors were quickly removed. Stomach and other gastrointestinal contents were removed and the urinary bladder was emptied. A 0.1 mL sample of blood was also collected. Each organ was weighed, and the tissue radioactivity was measured with an automated γ counter (1,282 Compugamma CS, Pharmacia/LKBNuclear, Inc.). The %ID/g was calculated by

comparison with samples of a standard dilution of the initial dose. All measurements were corrected for decay.

PET and CT imaging

A single NOD-SCID mouse implanted with PSMA+ PC3 PIP and PSMA− PC3 flu xenografts was used for imaging. The mouse was anesthetized with 3% isoflurane in oxygen for induction and maintained under 1.5% isoflurane in oxygen at a flow rate of 0.8 L/min. Then the mouse was placed in the prone position on the gantry of a GE eXplore VISTA small animal PET scanner (GE Healthcare) and injected intravenously with 0.38 mCi (14.1 MBq) [^{18}F]**3** in 200 μL of PBS. The images were acquired as a pseudo-dynamic scan, that is, a sequence of successive whole-body images were acquired in 2 bed positions. The dwell time at each position was 1 minute such that a given bed position (or mouse organ) was revisited every 3 minutes. An energy window of 250 to 700 keV was used. Images were reconstructed using the FORE/2D-OSEM method (1 iteration, 16 subsets) and included correction for radioactive decay, scanner dead time, and scattered radiation. After PET imaging the mobile mouse holder was placed on the gantry of an X-SPECT (Gamma Medica Ideas) small animal imaging device to acquire the corresponding CT. Animals were scanned over a 8.9-cm field-of-view using a 230 μA, 75 kVp beam. The PET and CT data were then coregistered using NIH AMIDE software (http://amide.sourceforge.net/).

Radiation dosimetry

The human dosimetry values were obtained using the mouse biodistribution data. The mouse organ activity concentrations in %ID/g were converted to the human %ID/organ by setting the ratio of organ %ID/g to whole-body %ID/g in the mouse equal to that in humans and then solving for the human %ID/organ; the adult male phantom organ masses listed in the OLINDA/EXM 1.0 were used for the conversion (64). The human source organ time-activity curves were fitted using a monoexponential function. Because the biodistribution data were radioactive decay corrected, only the biological removal constants were obtained from the curve fits, and the physical decay constant for ^{18}F was added in obtaining the time-integrated activity coefficients (TIAC). The source organ TIACs in MBq-h/MBq were entered in the OLINDA/EXM 1.0 for the dose calculations. The dynamic voiding bladder model was used to obtain the TIAC for the urinary bladder contents. The whole-body clearance half-life (obtained as sum of sampled tissues, excluding the tumors) was used as half-life to describe urinary bladder filling. All radioactivity was assumed eliminated *via* the urine. A 1 hour voiding interval was assumed.

Disclosure of Potential Conflicts of Interest

No potential conflicts of interest were disclosed.

Acknowledgments

We thank CA92871 and CA134675 for financial support. We also thank James Fox for performing the imaging studies and Gilbert Green and Jianhua Yu for excellent technical support.

The costs of publication of this article were defrayed in part by the payment of page charges. This article must therefore be hereby marked *advertisement* in accordance with 18 U.S.C. Section 1734 solely to indicate this fact.

Received May 27, 2011; revised September 6, 2011; accepted September 28, 2011; published OnlineFirst October 31, 2011.

References

1. Jemal A, Siegel R, Xu J, Ward E. Cancer statistics, 2010. CA Cancer J Clin 2010;60:277–300.
2. Ross JS, Sheehan CE, Fisher HA, Kaufman RP Jr, Kaur P, Gray K, et al. Correlation of primary tumor prostate-specific membrane antigen expression with disease recurrence in prostate cancer. Clin Cancer Res 2003;9:6357–62.
3. Perner S, Hofer MD, Kim R, Shah RB, Li H, Moller P, et al. Prostate-specific membrane antigen expression as a predictor of prostate cancer progression. Human Pathol 2007;38:696–701.
4. Horoszewicz JS, Kawinski E, Murphy GP. Monoclonal antibodies to a new antigenic marker in epithelial prostatic cells and serum of prostatic cancer patients. Anticancer Res 1987;7:927–35.
5. Smith-Jones PM, Vallabhajosula S, Navarro V, Bastidas D, Goldsmith SJ, Bander NH. Radiolabeled monoclonal antibodies specific to the extracellular domain of prostate-specific membrane antigen: preclinical studies in nude mice bearing LNCaP human prostate tumor. J Nucl Med 2003;44:610–7.
6. Evans MJ, Smith-Jones PM, Wongvipat J, Navarro V, Kim S, Bander NH, et al. Noninvasive measurement of androgen receptor signaling with a positron-emitting radiopharmaceutical that targets prostate-specific membrane antigen. Proc Natl Acad Sci U S A 2011;108:9578–82.
7. Pomper MG, Musachio JL, Zhang J, Scheffel U, Zhou Y, Hilton J, et al. 11C-MCG: synthesis, uptake selectivity, and primate PET of a probe for glutamate carboxypeptidase II (NAALADase). Mol Imaging 2002;1:96–101.
8. Foss CA, Mease RC, Fan H, Wang Y, Ravert HT, Dannals RF, et al. Radiolabeled small-molecule ligands for prostate-specific membrane antigen: *in vivo* imaging in experimental models of prostate cancer. Clin Cancer Res 2005;11:4022–8.
9. Mease RC, Dusich CL, Foss CA, Ravert HT, Dannals RF, Seidel J, et al. N-[N-[(S)-1,3-dicarboxypropyl]carbamoyl]-4-[18F]fluorobenzyl-L-cysteine, [18F]DCFBC: a new imaging probe for prostate cancer. Clin Cancer Res 2008;14:3036–43.
10. Banerjee SR, Foss CA, Castanares M, Mease RC, Byun Y, Fox JJ, et al. Synthesis and evaluation of technetium-99m- and rhenium-labeled inhibitors of the prostate-specific membrane antigen (PSMA). J Med Chem 2008;51:4504–17.
11. Chen Y, Foss CA, Byun Y, Nimmagadda S, Pullambhatla M, Fox JJ, et al. Radiohalogenated prostate-specific membrane antigen (PSMA)-based ureas as imaging agents for prostate cancer. J Med Chem 2008;51:7933–43.
12. Chen Y, Dhara S, Banerjee SR, Byun Y, Pullambhatla M, Mease RC, et al. A low molecular weight PSMA-based fluorescent imaging agent for cancer. Biochem Biophys Res Commun 2009;390:624–9.
13. Banerjee SR, Pullambhatla M, Byun Y, Nimmagadda S, Green G, Fox JJ, et al. 68Ga-labeled inhibitors of prostate-specific membrane antigen (PSMA) for imaging prostate cancer. J Med Chem 2010;53:5333–41.
14. Hillier SM, Maresca KP, Femia FJ, Marquis JC, Foss CA, Nguyen N, et al. Preclinical evaluation of novel glutamate-urea-lysine analogues that target prostate-specific membrane antigen as molecular imaging pharmaceuticals for prostate cancer. Cancer Res 2009;69:6932–40.

15. Joyal JL, Barrett JA, Marquis JC, Chen J, Hillier SM, Maresca KP, et al. Preclinical evaluation of an 131I-labeled benzamide for targeted radiotherapy of metastatic melanoma. Cancer Res 2010;70:4045–53.
16. Kularatne SA, Zhou Z, Yang J, Post CB, Low PS. Design, synthesis, and preclinical evaluation of prostate-specific membrane antigen targeted (99m)Tc-radioimaging agents. Mol Pharm 2009;6:790–800.
17. Liu T, Wu LY, Kazak M, Berkman CE. Cell-Surface labeling and internalization by a fluorescent inhibitor of prostate-specific membrane antigen. Prostate 2008;68:955–64.
18. Lapi SE, Wahnishe H, Pham D, Wu LY, Nedrow-Byers JR, Liu T, et al. Assessment of an 18F-labeled phosphoramidate peptidomimetic as a new prostate-specific membrane antigen-targeted imaging agent for prostate cancer. J Nucl Med 2009;50:2042–8.
19. Kwok A, Wang Y, Du Y, Tsui B, Pomper M. Physical phantom evaluation of the efficiency of reconstruction and compensation methods on quantitative SPECT prostate imaging. Annual Meeting of the Society of Nuclear Medicine. Washington D.C.: 2007. p. 471P.
20. DeGrado TR, Baldwin SW, Wang S, Orr MD, Liao RP, Friedman HS, et al. Synthesis and evaluation of (18)F-labeled choline analogs as oncologic PET tracers. J Nucl Med 2001;42:1805–14.
21. Bauman G, Belhocine T, Kovacs M, Ward A, Beheshti M, Rachinsky I. (18)F-fluorocholine for prostate cancer imaging: a systematic review of the literature. Prostate Cancer Prostatic Dis 2011; doi: 10.1038/pcan.2011.35. [Epub ahead of print].
22. Jadvar H. Prostate cancer: PET with 18F-FDG, 18F- or 11C-acetate, and 18F- or 11C-choline. J Nucl Med 2011;52:81–9.
23. Oyama N, Akino H, Kanamaru H, Suzuki Y, Muramoto S, Yonekura Y, et al. 11C-acetate PET imaging of prostate cancer. J Nucl Med 2002;43:181–6.
24. Morris MJ, Scher HI. (11)C-acetate PET imaging in prostate cancer. Eur J Nucl Med Mol Imaging 2007;34:181–4.
25. Schuster DM, Votaw JR, Nieh PT, Yu W, Nye JA, Master V, et al. Initial experience with the radiotracer anti-1-amino-3-18F-fluorocyclobutane-1-carboxylic acid with PET/CT in prostate carcinoma. J Nucl Med 2007;48:56–63.
26. Elsasser-Beile U, Reischl G, Wiehr S, Buhler P, Wolf P, Alt K, et al. PET imaging of prostate cancer xenografts with a highly specific antibody against the prostate-specific membrane antigen. J Nucl Med 2009;50:606–11.
27. Holland JP, Divilov V, Bander NH, Smith-Jones PM, Larson SM, Lewis JS. 89Zr-DFO-J591 for immunoPET of prostate-specific membrane antigen expression *in vivo*. J Nucl Med 2010;51:1293–300.
28. Nanus DM, Milowsky MI, Kostakoglu L, Smith-Jones PM, Vallabahajosula S, Goldsmith SJ, et al. Clinical use of monoclonal antibody HuJ591 therapy: targeting prostate specific membrane antigen. J Urol 2003;170:S84–8; discussion S8–9.
29. Milowsky MI, Nanus DM, Kostakoglu L, Sheehan CE, Vallabhajosula S, Goldsmith SJ, et al. Vascular targeted therapy with anti-prostate-specific membrane antigen monoclonal antibody J591 in advanced solid tumors. J Clin Oncol 2007;25:540–7.
30. Cho SY, Mease RC, Holt D, Dannals RF, Eisenberger M, Rodriguez R, et al. Initial clinical assessment of DCFBC-PET for metastatic prostate cancer (PCa). Annual Meeting of the Society of Nuclear Medicine. San Antonio, TX: 2011. p. 12P.
31. Olberg DE, Arukwe JM, Grace D, Hjelstuen OK, Solbakken M, Kindberg GM, et al. One step radiosynthesis of 6-[(18)F]fluoronicotinic acid 2,3,5,6-tetrafluorophenyl ester ([(18)F]F-Py-TFP): a new prosthetic group for efficient labeling of biomolecules with fluorine-18. J Med Chem 2010;53:1732–40.
32. Kozikowski AP, Zhang J, Nan F, Petukhov PA, Grajkowska E, Wroblewski JT, et al. Synthesis of urea-based inhibitors as active site probes of glutamate carboxypeptidase II: efficacy as analgesic agents. J Med Chem 2004;47:1729–38.
33. Silver DA, Pellicer I, Fair WR, Heston WD, Cordon-Cardo C. Prostate-specific membrane antigen expression in normal and malignant human tissues. Clin Cancer Res 1997;3:81–5.
34. Slusher BS, Tsai G, Yoo G, Coyle JT. Immunocytochemical localization of the N-acetyl-aspartyl-glutamate (NAAG) hydrolyzing enzyme N-acetylated alpha-linked acidic dipeptidase (NAALADase). J Comp Neurol 1992;315:217–29.
35. Rajasekaran AK, Anilkumar G, Christiansen JJ. Is prostate-specific membrane antigen a multifunctional protein? Am J Physiol Cell Physiol 2005;288:C975–81.
36. Ghosh A, Heston WD. Tumor target prostate specific membrane antigen (PSMA) and its regulation in prostate cancer. J Cell Biochem 2004;91:528–39.
37. Zaheer A, Cho SY, Pomper MG. New agents and techniques for imaging prostate cancer. J Nucl Med 2009;50:1387–90.
38. Kurhanewicz J, Vigneron D, Carroll P, Coakley F. Multiparametric magnetic resonance imaging in prostate cancer: present and future. Curr Opin Urol 2008;18:71–7.
39. Mease RC. Radionuclide based imaging of prostate cancer. Curr Top Med Chem 2010;10:1600–16.
40. Chandran SS, Banerjee SR, Mease RC, Pomper MG, Denmeade SR. Characterization of a targeted nanoparticle functionalized with a urea-based inhibitor of prostate-specific membrane antigen (PSMA). Cancer Biol Ther 2008;7:974–82.
41. Gao X, Cui Y, Levenson RM, Chung LW, Nie S. *In vivo* cancer targeting and imaging with semiconductor quantum dots. Nat Biotechnol 2004;22:969–76.
42. Bagalkot V, Zhang L, Levy-Nissenbaum E, Jon S, Kantoff PW, Langer R, et al. Quantum dot-aptamer conjugates for synchronous cancer imaging, therapy, and sensing of drug delivery based on bi-fluorescence resonance energy transfer. Nano Lett 2007;7:3065–70.
43. Vorhies JS, Nemunaitis JJ. Nucleic acid aptamers for targeting of shRNA-based cancer therapeutics. Biologics 2007;1:367–76.
44. Chang SS, Reuter VE, Heston WD, Bander NH, Grauer LS, Gaudin PB. Five different anti-prostate-specific membrane antigen (PSMA) antibodies confirm PSMA expression in tumor-associated neovasculature. Cancer Res 1999;59:3192–8.
45. Chang SS, O'Keefe DS, Bacich DJ, Reuter VE, Heston WD, Gaudin PB. Prostate-specific membrane antigen is produced in tumor-associated neovasculature. Clin Cancer Res 1999;5:2674–81.
46. Schulke N, Varlamova OA, Donovan GP, Ma D, Gardner JP, Morrissey DM, et al. The homodimer of prostate-specific membrane antigen is a functional target for cancer therapy. Proc Natl Acad Sci U S A 2003;100:12590–5.
47. Haffner MC, Kronberger IE, Ross JS, Sheehan CE, Zitt M, Muhlmann G, et al. Prostate-specific membrane antigen expression in the neovasculature of gastric and colorectal cancers. Human Pathol 2009;40:1754–61.
48. Wright GL Jr, Grob BM, Haley C, Grossman K, Newhall K, Petrylak D, et al. Upregulation of prostate-specific membrane antigen after androgen-deprivation therapy. Urology 1996;48:326–34.
49. Mostaghel EA, Page ST, Lin DW, Fazli L, Coleman IM, True LD, et al. Intraprostatic androgens and androgen-regulated gene expression persist after testosterone suppression: therapeutic implications for castration-resistant prostate cancer. Cancer Res 2007;67:5033–41.
50. Tran C, Ouk S, Clegg NJ, Chen Y, Watson PA, Arora V, et al. Development of a second-generation antiandrogen for treatment of advanced prostate cancer. Science 2009;324:787–90.
51. Dehdashti F, Picus J, Michalski JM, Dence CS, Siegel BA, Katzenellenbogen JA, et al. Positron tomographic assessment of androgen receptors in prostatic carcinoma. Eur J Nucl Med Mol Imaging 2005;32:344–50.
52. Dehdashti F, McGuire AH, Van Brocklin HF, Siegel BA, Andriole DP, Griffeth LK, et al. Assessment of 21-[18F]fluoro-16 alpha-ethyl-19-norprogesterone as a positron-emitting radiopharmaceutical for the detection of progestin receptors in human breast carcinomas. J Nucl Med 1991;32:1532–7.
53. Elsasser-Beile U, Reischl G, Wiehr S, Buhler P, Wolf P, Alt K, et al. PET imaging of prostate cancer xenografts with a highly specific antibody against the prostate-specific membrane antigen. J Nucl Med 2009;50:606–11.
54. Alt K, Wiehr S, Ehrlichmann W, Reischl G, Wolf P, Pichler BJ, et al. High-resolution animal PET imaging of prostate cancer xenografts with three different 64Cu-labeled antibodies against native cell-adherent PSMA. Prostate 2010;70:1413–21.
55. Rockey WM, Huang L, Kloepping KC, Baumhover NJ, Giangrande PH, Schultz MK. Synthesis and radiolabeling of chelator-RNA aptamer

bioconjugates with copper-64 for targeted molecular imaging. Bioorg Med Chem 2011;19:4080–90.
56. Kozikowski AP, Nan F, Conti P, Zhang J, Ramadan E, Bzdega T, et al. Design of remarkably simple, yet potent urea-based inhibitors of glutamate carboxypeptidase II (NAALADase). J Med Chem 2001;44:298–301.
57. Malik N, Machulla HJ, Solbach C, Winter G, Reske SN, Zlatopolskiy B. Radiosynthesis of a new PSMA targeting ligand ([18F]FPy-DUPA-Pep). Appl Radiat Isot 2011;69:1014–8.
58. Davis MI, Bennett MJ, Thomas LM, Bjorkman PJ. Crystal structure of prostate-specific membrane antigen, a tumor marker and peptidase. Proc Natl Acad Sci U S A 2005;102:5981–6.
59. Mesters JR, Barinka C, Li W, Tsukamoto T, Majer P, Slusher BS, et al. Structure of glutamate carboxypeptidase II, a drug target in neuronal damage and prostate cancer. Embo J 2006;25:1375–84.
60. Barinka C, Byun Y, Dusich CL, Banerjee SR, Chen Y, Castanares M, et al. Interactions between human glutamate carboxypeptidase II and urea-based inhibitors: structural characterization. J Med Chem 2008; 51:7737–43.
61. Wu P, Kudrolli TA, Chowdhury WH, Liu MM, Rodriguez R, Lupold SE. Adenovirus targeting to prostate-specific membrane antigen through virus-displayed, semirandom peptide library screening. Cancer Res 2010;70:9549–53.
62. Cheng Y, Prusoff WH. Relationship between the inhibition constate (K1) and the concentration of inhibitor which causes 50 percent inhibition (I50) of an enzymatic reaction. Biochem Pharmcol 1973;22: 3099–108.
63. Cheng HC. determination of KB or Ki from IC_{50}. A closer look at the Cheng-Prusoff equation, the Schild plot and related power equations. J Pharmacol Toxicol Methods 2001;46:61–71.
64. Stabin MG, Sparks RB, Crowe E. OLINDA/EXM: the second-generation personal computer software for internal dose assessment in nuclear medicine. J Nucl Med 2005;46:1023–7.